SPECIAL SECTION

The use of DSC curves and Kronmüller theory to study the level of structural defects of Fe-based bulk amorphous alloys

Bartłomiej JEŻ[1] [ORCID]* and Marcin NABIAŁEK[2]

[1] Department of Technology and Automation, Faculty of Mechanical Engineering and Computer Science, Czestochowa University of Technology,
al. Armii Krajowej 19c, 42-200 Czestochowa, Poland
[2] Department of Physics, Faculty of Production Engineering and Materials Technology, Czestochowa University of Technology,
al. Armii Krajowej 19, 42-200 Częstochowa, Poland

Abstract. This article presents the results of tests carried out on rapidly-quenched Fe-based alloys. The alloys were made using an injection-casting method. The actual structure of the alloys was also studied using an indirect method, based on H. Kronmüller's theorem. Based on analysis of the primary magnetization curves, in accordance with the aforementioned theory, it was found that Mo causes a change in internal regions associated with changes in the direction of the magnetization vector. The evolution of thermal properties with increasing volume of Mo has been confirmed by the DSC curves. Addition of Mo, at the expense of the Nb component, results in changes to the crystallization process (i.e. the crystallization onset temperature and number of stages). The study showed that the addition of Mo at the expense of Nb reduces the glass-forming ability. Based on DSC analysis, free volumes were determined for the alloys tested. These values were compared with the analysis of primary magnetization curves. It was found that the DSC curves can be used to indirectly describe the structure of amorphous alloys, similarly to the theory of approach to ferromagnetic saturation. This approach is new and can be used by many researchers in this field.

Key words: injection-casting method; bulk amorphous alloys; soft magnetic materials; free volume; structural defects.

1. INTRODUCTION

Amorphous, metal-based alloys have been studied for several decades to date [1–3]. These materials are characterized by different properties when compared with those of their crystalline counterparts [4, 5]; this fact is related to the structure of the alloys. Disorder, which determines both the mechanical and magnetic properties of amorphous alloys, is extremely difficult to describe. So-called good soft-magnetic properties (i.e. low coercive field value and high saturation magnetization [6–10]) are influenced by the distances between magnetic atoms, the number of magnetic neighbors and the arrangement of atoms. Moreover, during the solidification process of the alloy, energetically favored regions and structural defects are created. In amorphous materials, defects are present in the form of "free volumes" and quasi-dislocational dipoles [11–13]. Free volumes are equivalent to the point defects found in crystalline materials. A point defect, occurring in an amorphous matrix, is a free space which is larger than the smallest alloying element. Quasi-dislocational dipoles are conglomerates of at least a few free volumes.

The magnetization process of alloys with an amorphous structure is dependent largely on structural defects. The magnetization vector is extremely sensitive to any inhomogeneities occurring in the volume of the material. During the magnetiza-

tion process, the magnetization vector near structural defects is disturbed, and this effect is visible on the primary magnetization curves. Magnetization in high values of the external magnetic field does not immediately reach saturation values. At a certain value of magnetic field strength, the increase in magnetization is slowed down significantly. This area on the curve is called "the approach to ferromagnetic saturation". According to H. Kronmüller [14–18], magnetization in this area can be described by the following equation:

$$\mu_0 M(H) = \mu_0 M_s \left[1 - \frac{a_{0.5}}{(\mu_0 H)^{0.5}} - \frac{a_1}{(\mu_0 H)^1} - \frac{a_2}{(\mu_0 H)^2} \right] + b(\mu_0 H)^{0.5}, \tag{1}$$

where: M_s – spontaneous magnetization, μ_0 – magnetic permeability of a vacuum, H – magnetic field, a_i ($i = 1/2, 1, 2$) – angular coefficients of the linear fit, which corresponds to the free volumes and linear defects, b – slope of the linear fit corresponding to the thermally-induced suppression of spin-waves by a magnetic field of high intensity.

Parameters $a_{1/2}$, a_1 and a_2 can be determined from analysis of the primary magnetization curve. These factors are described by the following relationships:

$$\frac{a_{0.5}}{(\mu_0 H)^{0.5}} = \mu_0 \frac{3}{20 A_{\mathrm{ex}}} \left(\frac{1+r}{1-r} \right)^2$$
$$\cdot G^2 \lambda_s^2 (\Delta V)^2 N \left(\frac{2 A_{\mathrm{ex}}}{\mu_0 M_s} \right)^{0.5} \frac{1}{(\mu_0 H)^{0.5}}, \tag{2}$$

$$\frac{a_1}{\mu_0 H} = 1.1\mu_0 \frac{G^2\lambda_s^2}{(1-v)^2}\frac{Nb_{\text{eff}}}{M_s A_{\text{ex}}}D_{\text{dip}}^2\frac{1}{\mu_0 H}, \qquad (3)$$

$$\frac{a_2}{\mu_0 H^2} = 0.456\mu_0 \frac{G^2\lambda_s^2}{(1-v)^2}\frac{Nb_{\text{eff}}}{M_s^2}D_{\text{dip}}^2\frac{1}{(\mu_0 H)^2}, \qquad (4)$$

where: ΔV – the change in volume due to the occurrence of a point defect characterized by a bulk density of N, A_{ex} – exchange constant, G – transverse elastic shear modulus, r – Poisson's ratio, λ_s – magnetostriction constant.

The process of magnetization in a magnetic field greater than the anisotropy field is associated with the damping of thermally-induced spin-waves [19]. This process is described using the spin-wave stiffness parameter D_{spf}. This parameter is related to the b factor in the following manner:

$$b = 3.54g\mu_0\mu_B\left(\frac{1}{4\pi D_{\text{spf}}}\right)^{1.5}kT(g\mu_B)^{0.5}, \qquad (5)$$

where: k – Boltzmann's constant, μ_B – Bohr magneton, g – gyromagnetic factor.

In the literature, relations between thermal stability of amorphous alloys and their magnetic properties are found. The increase in the values of characteristic temperatures T_g, T_x and ΔT_x is associated with a decrease in saturation magnetization and an increase in the value of the coercive field depending on the chemical composition of the alloy [20]. There are also works showing inverse [21] relationships.

The measurement of DSC curves is commonly used for amorphous alloys. Typically, DSC curves are only used to describe the crystallization process of these alloys. Based on these curves, it is possible to determine the free volumes present in the alloy. This fact can be related to the description of the structure defects determined according to H. Kronmüller's theory.

One of the primary aims of this study was to determine structure defects using H. Kronmüller's theory and DSC curves. The additional purpose of the study was to determine the structural and magnetic properties of novel bulk amorphous alloys that are based on iron.

2. MATERIALS AND METHODS

The chemical compositions of the alloys were selected on the basis of criteria formulated by A. Inoue: (1) multi-component alloy, (2) negative heat of mixing, and (3) relatively large differences in the lengths of the atomic radii of the main alloying components [22–24]. Figure 1 presents a diagram of the heat of mixing and differences in the lengths of the atomic radii of the alloying elements.

The designed chemical compositions comply with A. Inoue's criteria, with the exception of the positive heat of the Mo–Y and Nb–Y pairs of atoms, and the relatively minor differences in the lengths of the atomic radii for the Mo-Fe and Mo–Nb pairs.

Polycrystalline alloys with the following chemical compositions: $Fe_{70}B_{20}Y_5Nb_{5-x}Mo_x$ (where: $x = 0, 1, 2, 3, 4, 5$) were produced in an arc furnace. Each load mix was melted on a water-cooled copper plate under protective argon atmosphere.
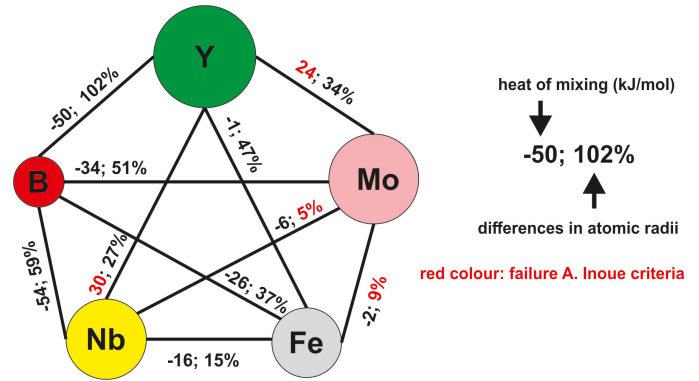

Fig. 1. Heat of mixing and differences in the atomic radii of the components for the investigated alloys (red color means failure to meet the A. Inoue criterion)

The melting process was repeated seven times, in order to achieve homogenization of the composition; and, after each melting process, the ingots were physically inverted. Each remelting process was preceded by melting a titanium getter. The initial ingots, each of 10 grams in weight, were divided into smaller pieces and subjected to mechanical and ultrasonic cleaning processes. Rapidly-quenched alloy samples were prepared using an injection-casting method, with a cooling rate of up to 10^3 K/s. Before the injection process, the copper mold is cooled with water for several dozen seconds. For this reason, the temperature of the mold is equal to the temperature of the feed water and amounts approximately to 17–20°C. The production process was carried out under the protective atmosphere of argon. The polycrystalline material was placed in a quartz crucible and melted using induction heating. The liquid alloy was forced into a water-cooled copper mold. The resulting samples, in the form of plates with the following dimensions: 10 mm × 10 mm × 0.5 mm, were subjected to mechanical and ultrasonic cleaning. Powdered alloy samples were tested. The powders were obtained by means of low-energy crushing in an agate mortar in toluene. This procedure ensures obtaining objective test results. The alloy structure was examined using X-ray diffractometry; a BRUKER D8 Advance diffractometer, equipped with a CuKα lamp and a semiconductor meter, was used for this investigation. The tests were carried out on samples representing the whole volume of each material (i.e. samples in the form of powders). The samples were exposed for 7 seconds per 0.02° measuring step. The measurement was carried out in the range of the 2θ angle from 30° to 100°.

Measurements of thermal stability were performed using a Netzsch STA calorimeter (STA 449 F5 Jupiter by NETZSCH). The samples were in the form of powders, and the heating rate was 10 K/min.

Magnetic properties were measured using a LakeShore vibrating-sample magnetometer (VSM). Primary magnetization curves were recorded. The measurements were carried out over a range of magnetic field strengths extending up to 2T at room temperature. Analysis of the primary magnetization curves was carried out according to H. Kronmüller's theory.

2

Bull. Pol. Acad. Sci. Tech. Sci., vol. 71, no. 2, p. e144613, 2023

3. RESULTS

Figure 2 shows the X-ray diffraction patterns which were obtained for the samples produced.
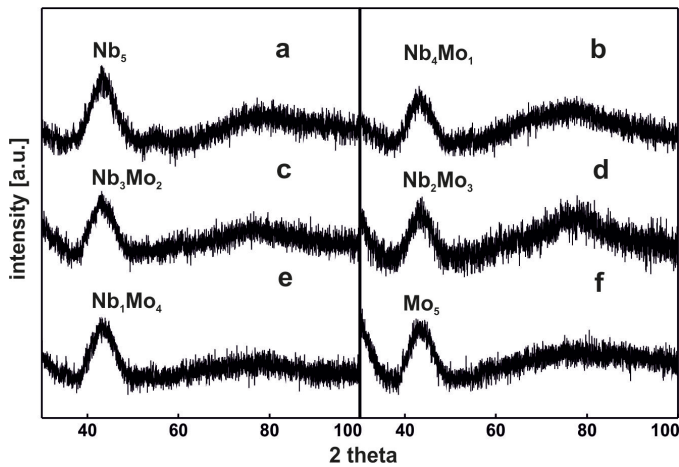
Fig. 2. X-ray diffraction images for the $Fe_{70}B_{20}Y_5Nb_{5-x}Mo_x$ alloys:
a) Nb_5, b) Nb_4Mo_1, c) Nb_3Mo_2, d) Nb_2Mo_3, e) Nb_1Mo_4, f) Mo_5

The recorded X-ray diffraction images were found to be typical for amorphous materials: only wide diffused maxima are visible. This maximum is related to the reflection of X-rays from atoms chaotically distributed in the volume of the alloy.

Thermal stability is a very important parameter of functional materials for use in electrical engineering. Figure 3 represents thermograms for the investigated alloys. Figure 3 depicted the DSC curves of the mentioned alloys at various heating rates of (10, 20, 30, 40 K/min) from ambient temperature up to 1200°C. According to Fig. 3, all samples show a multi-step crystallization process and one endothermic peak. The characteristic temperatures determined for the investigated alloys are listed in Table 1. As you know, the temperature most commonly used as the glass transition temperature (T_g) is measured by the point of intersection of the tangent drawn at the point of the greatest slope on the transition curve with the extrapolated baseline prior to the transition (the start of T_g (Fig. 3)) [25, 26]. Also, the onset crystallization temperature (T_{x1}) characterizes the start of crystallization on heating. This temperature is calculated by the intersection of the extrapolated linear section of the rising peak edge with the baseline extrapolated from temperatures above the peak [27]. In addition, all critical temperatures, including glass transition temperature (T_g), onset of crystallization temperature (T_{x1}), secondary crystallization temperature (T_{x2}), melting temperature (T_m) and liquid alloy temperature (T_l), are specified in the DSC curves.

Based on the analysis of data contained in Table 1, it could be stated that the value of temperature T_g is sensitive to the Nb content within the alloy. With a decrease in the quantity of Nb to the value of 1%, the value of T_g is increasing. A total absence of Nb in the alloy results in a rapid decrease in T_g, when compared with the alloy containing 1% of Nb. The monotonic decrease of the T_{x2} values is related to the increase in the quantity of Mo in the volume of the alloy. This helps explain the glass-forming ability of the investigated BMGs. According to the data
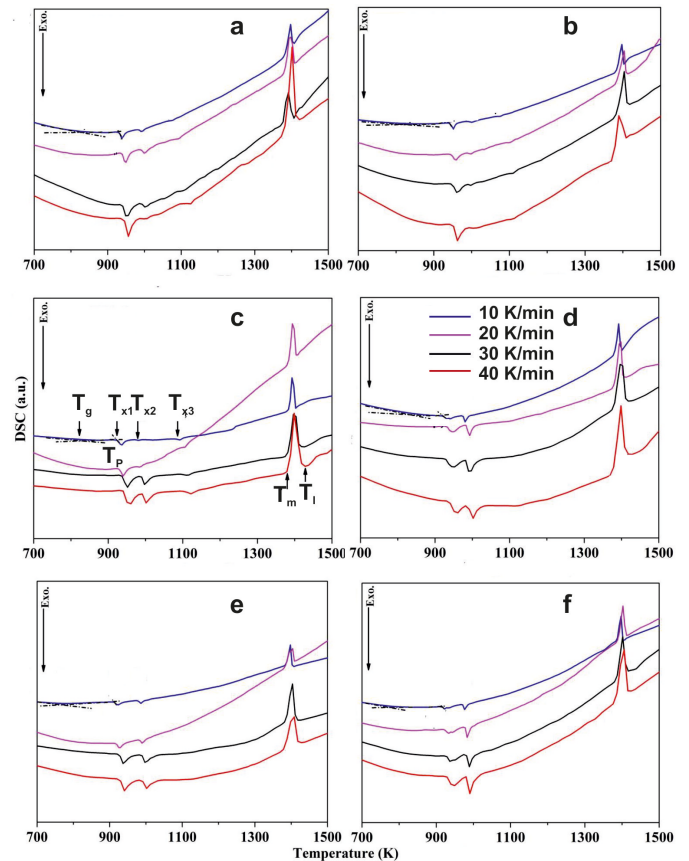

Fig. 3. DSC curves for the $Fe_{70}B_{20}Y_5Nb_{5-x}Mo_x$ alloys at various heating rates (10, 20, 30, and 40 K/min): a) Nb_5, b) Nb_4Mo_1, c) Nb_3Mo_2, d) Nb_2Mo_3, e) Nb_1Mo_4, f) Mo_5

Table 1
Thermal properties of $Fe_{70}B_{20}Y_5Nb_{5-x}Mo_x$ alloys at a heating rate of 20 K/min

Sample	Critical temperature [K]					
	T_g	T_{x1}	T_{x2}	T_{x3}	T_m	T_l
Nb_5	852.3	938.9	986.9	1079.7	1378.1	1402.6
Nb_4Mo_1	850.2	935.1	983.8	1085.9	1377.8	1407.0
Nb_3Mo_2	848.5	923.4	981.0	1096.7	1383.1	1402.0
Nb_2Mo_3	847.4	922.2	978.2	–	1383.0	1402.7
Nb_1Mo_4	845.0	918.6	975.9	–	1377.3	1402.0
Mo_5	842.7	914.1	971.4	–	1383.0	1402.7

extracted from the alpha curve, some criteria, such as the supercooled liquid region ($\Delta T_x = T_x - T_g$) [28], $T_{rg} = T_g/T_l$ [29], $\gamma = T_x/(T_g + T_l)$ [30], $\delta = T_x/(T_l - T_g)$ [31], were calculated and are depicted in Table 2. As shown in Table 2, these alloys feature outstanding supercooled liquid regions as compared with other Fe-based BMGs [32, 33]. Moreover, replacement of Mo with Nb leads to an increase in glass-forming ability (GFA). Hence, these criteria have a similar trend to the results obtained

Bull. Pol. Acad. Sci. Tech. Sci., vol. 71, no. 2, p. e144613, 2023

3

for thermal stability of these alloys. Also, activation energy is used to investigate the thermal energy activation required for atomic motion and thermal stability of materials.

Table 2
Thermal properties of $Fe_{70}B_{20}Y_5Nb_{5-x}Mo_x$ BMGs at a heating rate of 20 K/min

Sample	Criteria			E (kJ/mol)		ΔG_c	Free volume
	ΔT_x	T_{rg}	γ	E_p	E_x	(kJ/mol)	(J/g)
Nb_5	86.6	0.61	0.43	775.99	475.42	1.54	117
Nb_4Mo_1	84.9	0.60	0.42	601.35	449.81	1.64	125
Nb_3Mo_2	75.9	0.60	0.42	461.17	424.84	1.75	164
Nb_2Mo_3	74.8	0.59	0.41	423.84	407.21	2.14	199
Nb_1Mo_4	72.6	0.58	0.40	394.74	316.04	2.38	221
Mo_5	71.3	0.57	0.40	283.59	305.94	1.98	228

Therefore, in this study, the value of activation energy (E_p) related to the first step of crystallization based on (7) can be measured from the Kissinger–Akahira–Sunose (KAS) method [34], which is obtained based on the integral of the iso-conversional method (Fig. 4).

$$\ln\left(\frac{\beta}{T^2}\right) = \text{constant} - E_p/RT, \qquad (6)$$

where: β is the linear heating rate (K/min); T is the absolute temperature (K); R is the general gas constant (J/mol K); and E is activation energy (kJ/mol). To calculate apparent activation energy, the plot $\ln(\beta/T^2)$ vs. $1000/T_p$ should be a straight line whose slope can be used.

Therefore, for accuracy of the results related to the study of glass-forming ability, the activation energy of the first peak of the crystallization of the mentioned alloys was obtained and is reported in Table 2. As shown, the value of activation energy increases with the replacement of Mo with Nb. In other words, thermal stability increases and crystallization is delayed, which is consistent with the other results (crystallization retarded in time and occurring at a higher temperature). The results revealed that with the replacement of Mo with Nb, atomic mobility decreases and thermal stability increases.

Also, the Gibbs free energy is an important parameter in the nucleation theory of crystallization of multicomponent undercooled systems. This parameter described the temperature dependence of heat capacity, which is based on the assumption that the term undercooling degree ($\Delta T = T_m - T$) is small. Also, from the thermodynamic point of view, free energy can be a good indicator of the glass-forming ability [35]. Therefore, it is reported that the Gibbs free energy difference (ΔG_c) between the undercooled melt and the corresponding competing crystalline phases in a specified alloy system is an accuracy criterion for obtaining thermal stability of the amorphous matrix.

A smaller ΔG_c indicates higher GFA [36]. The ΔG_c of the investigated alloys was calculated using (8) as modified by Bat-

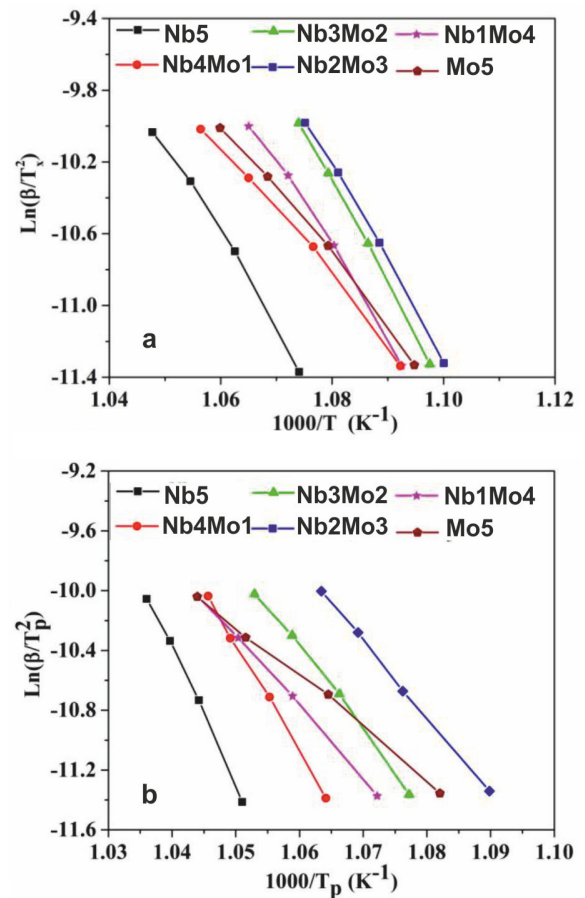**Fig. 4.** Plots of the: a) $\ln(\beta/T_p^2)$ vs. $1000/Tp$ related to the first crystallization stage of $Fe_{70}B_{20}Y_5Nb_{5-x}Mo_x$ BMGs by means of KAS method; b) $\ln(\beta/T_x^2)$ vs. $1000/T_x$ related to the onset crystallization stage of $Fe_{70}B_{20}Y_5Nb_{5-x}Mo_x$ BMGs by means of KAS method

tezzati and Garrone [37].

$$\Delta G_c = \frac{\Delta H_f \Delta T}{T_m}\tau\Delta S_f\left[\Delta T - T\ln\left(\frac{T_m}{T}\right)\right], \qquad (7)$$

where: ΔH_f is the fusion enthalpy (kJ/mol); ΔT equals $T_m - T$ (K); ΔS_f equals $\Delta H_f/T_m$ (kJ/molK); and τ is the proportionality coefficient – usually taken as 0.8 for metallic glass-forming liquids. In addition, $0.8\,T_m$ is usually selected as T [38].

In this paper, the ΔG_c parameters for the Nb_5 and Nb_1Mo_4 alloys are 1.51 and 2.21 kJ/mol, respectively, as shown in Table 2. Therefore, the obtained results are in good agreement with the thermal stability criteria. Furthermore, another method used for studying GFA is the free volume which is obtained with the enthalpy changes near the glass transition by using DSC curves. A smaller free volume with less atomic mobility leads to a higher GFA [39, 40]. Therefore, according to Table 2, the Nb_5 alloy has the highest thermal stability.

There is a distinct divide between the studied alloys: the first three alloys (featuring relatively small quantities of Mo) are characterized by the considerable contribution of primary crystallization, and the crystallization process takes place in three stages. The alloy with the 3% content of Mo is an alloy with a

"transitional" structure, in this case, the peaks indicative of the primary and secondary crystallization are similar in size, and the crystallization process occurs in two stages. For the cases in which there is a greater share of Mo as compared with Nb, the third crystallization peak – occurring at a temperature of approximately 1100 K for the alloys with Mo = 0 or 1% – disappears. The replacement of Mo with Nb results in a reduction in the crystallization onset temperature. The crystallization process consists of three stages; however, in this case, two stages are related to the primary crystallization. The occurrence of the two minima, located very close to each other, could indicate the presence of two distinct regions with amorphous structures, and slightly different chemical compositions. The presence of two different local short range orderings may result in the presence of two distinct values of temperature T_g.

The approach to ferromagnetic saturation was studied, based on magnetization measurements in strong magnetic fields. Figure 5 shows high-field magnetization curves for the tested alloys. For the Nb$_5$ alloy, in the range of the magnetizing field from 0.029 T to 0.047 T, a linear relationship for reduced magnetization is visible (Fig. 5a); this indicates that, in this range of the magnetizing field, point defects have a decisive impact on the magnetization process. A linear relationship is observed in the range of magnetic field induction from 0.05 T to 0.34 T (Fig. 5b), which shows that, in this range of the magnetic field, the process of magnetization occurs through microscopic rotation of magnetic moments near linear defects, for which the inverse of the exchange distance and dipole width are related. Similar relationships were observed for the Nb$_4$Mo$_1$ alloy (Fig. 5c, d). In the case of the Nb$_4$Mo$_1$ alloy, the magnetization process is also affected by the microscopic rotation of magnetic moments near defects (Fig. 5c) and linear defects: so-called quasi-dislocational dipoles (Fig. 5d). In the range of the magnetizing field from 0.035 T to 0.2 T for the Nb$_3$Mo$_2$ alloy (Fig. 5ea), and 0.038 T to 0.19 T for the Nb$_2$Mo$_3$ alloy (Fig. 5f), there is a linear relationship of $M/MS(\mu_0 H)^{-1}$. This means that the magnetization process for these alloys is influenced mainly by quasi-dislocational dipoles. In the magnetic

field induction range from 0.04 T to 0.085 T, a linear relationship is observed for the Nb$_1$Mo$_4$ alloy (Fig. 5g). This relationship indicates the existence of quasi-dislocational dipoles in the sample, for which the relationship is fulfilled. In the fields from 0.085 T to 0.17 T, a linear dependence of reduced magnetization was observed (Fig. 5h). This means that the magnetization process of this examined alloy is also affected by linear defects for which the relationship is fulfilled. In the case of the Mo$_5$ alloy, in the field range from 0.067 T to 0.21 T, a linear relationship was observed. This means that for this alloy, the magnetization process in the given range of fields is affected mainly by linear defects (Fig. 5i). Figure 6 presents magnetization curves as a function of $(\mu_0 H)^{1/2}$ for the investigated samples.

Above the so-called approach to magnetic saturation region, a further magnetization process is related with the damping of the thermally induced spin-waves (Holstein-Primakoff process). For the investigated alloys, the onset of this process could be observed at the value of external magnetic field from 0.21 to 0.34 T.

Based on the value of the b parameter of the fitting of the magnetization curves as a function of $(\mu_0 H)^{1/2}$, the spin-wave stiffness parameter D_{spf} was determined. Table 3 summarizes the results of the magnetic studies on the tested samples.

In the case of the Nb$_5$ and Nb$_4$Mo$_1$ alloys, the magnetization process is associated with the presence of both point and line defects in the sample ($D_{dip} < 1_H$). For the Nb$_3$Mo$_2$ and Nb$_2$Mo$_3$ alloys, the presence was detected of linear defects satisfying relationship (3). The magnetization of the Nb$_1$Mo$_4$ alloy is influenced by linear defects, satisfying both relationship (3) and relationship (4), while the magnetization process of the Mo$_5$ alloy only features the influence of linear defects with dimensions exceeding the exchange distance. On this basis, it can be concluded that alloys with a higher Nb content are characterized by higher atomic-packing density. These results are confirmed by calculations of ΔG_c and free volume (Table 2). Within the scope of the occurrence of the Holstein-Primakoff para-process, and on the basis of relationship (5), the spin-wave stiffness parameter D_{spf} was determined. The largest value of
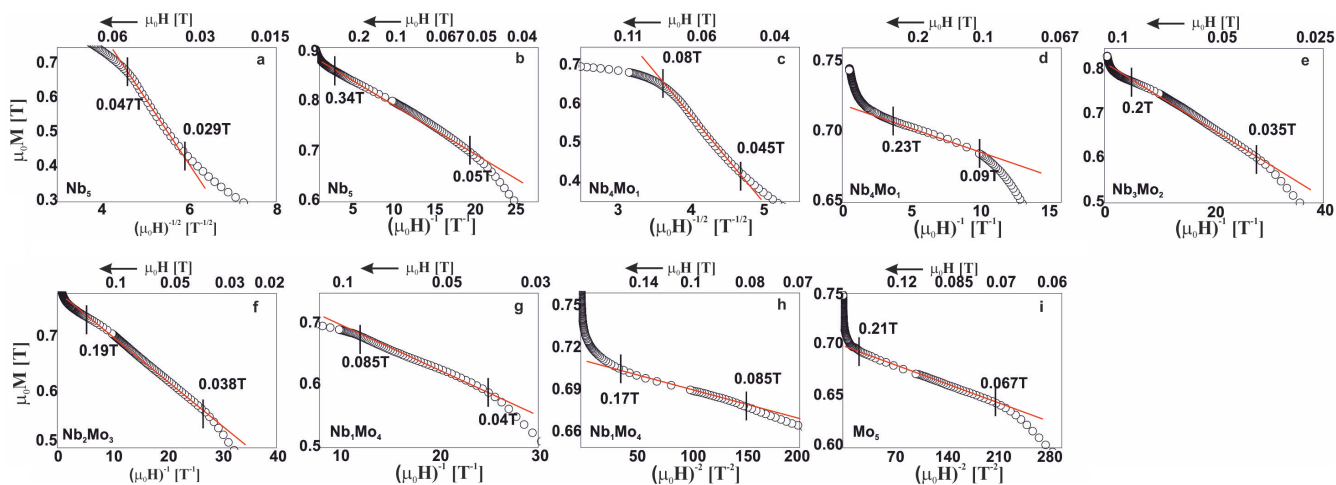

Fig. 5. Magnetization curves as a function of $(\mu_0 H)^{-1/2}$, $(\mu_0 H)^{-1}$ and $(\mu_0 H)^{-2}$ for the alloys: Nb$_5$: a) $(\mu_0 H)^{-1/2}$, b) $(\mu_0 H)^{-1}$; Nb$_4$Mo$_1$: c) $(\mu_0 H)^{-1/2}$, d) $(\mu_0 H)^{-1}$; Nb$_3$Mo$_2$: e) $(\mu_0 H)^{-1}$; Nb$_2$Mo$_3$: f) $(\mu_0 H)^{-1}$; Nb$_1$Mo$_4$: g) $(\mu_0 H)^{-1}$, h) $(\mu_0 H)^{-2}$; Mo$_5$: i) $(\mu_0 H)^{-2}$

Bull. Pol. Acad. Sci. Tech. Sci., vol. 71, no. 2, p. e144613, 2023

5
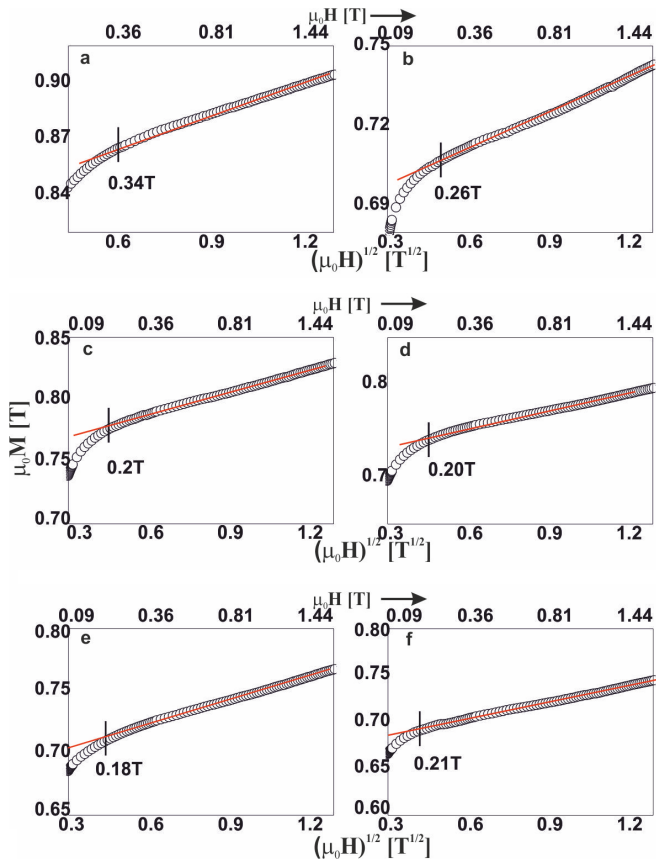
Fig. 6. Magnetization curves as a function of $(\mu_0 H)^{1/2}$ for the alloys: a) Nb_5, b) Nb_4Mo_1, c) Nb_3Mo_2, d) Nb_2Mo_3, e) Nb_1Mo_4, f) Y_5Mo_5

Table 3
Magnetic properties of the alloys: $Fe_{70}B_{20}Y_5Nb_{5-x}Mo_x$
(where: $x = 0, 1, 2, 3, 4, 5$)

Sample	Magnetic properties	Structural defects			D_{spf}
	M_s [T]	Point defects	$D_{dip} < l_H$	$D_{dip} > l_H$	[meVnm^2]
Nb_5	**0.9**	+	+		**46.5**
Nb_4Mo_1	**0.87**	+	+		**45.5**
Nb_3Mo_2	**0.83**		+		**44.8**
Nb_2Mo_3	**0.8**		+		**43.8**
Nb_1Mo_4	**0.77**		+	+	**43.4**
Mo_5	**0.75**			+	**42.9**

this parameter was found for the Nb_5 alloy sample; as the Mo content in a sample increases, a decrease is observed in the value of this parameter (Fig. 7).

This parameter is related to the number of magnetic neighbors and the mutual distances between them [41, 42]. A higher value of this parameter means that the atomic-packing density in the alloy is higher. With increasing Mo content, at the expense of Nb, a decrease was observed in the value of the satura-

Fig. 7. Relationships of magnetic properties and GFA parameters with Mo content

tion magnetization (Fig. 7). A similar relation was observed for the values of D_{spf}, T_{x1}, T_{x2}, T_g, ΔT_x, T_{rg}, γ, E_p and E_x (Fig. 7).

Structural relaxations lead to changes in the chemical order of alloys. The redistribution of elements within the volume of an alloy is strongly dependent on the composition of the alloy. In accordance with A. Inoue's criteria of negative heat of mixing and differences in atomic radii lengths, a certain relationship – confirming the test results – was observed for the studied alloys. The alloy without Mo fulfils A. Inoue's criteria, except for the positive heat of mixing the Nb–Y pairs of atoms. On the other hand, Molybdenum (Mo), is characterized by a minor difference in the lengths of atomic radii in relation to Fe, Nb and Y; which, according to A. Inoue, reduces the glass-forming ability. The reduction in the GFA is related directly to the re-

duction in viscosity in the solidification process, which in turn is associated with a reduction in the energy of the entire system. In this case, with the replacement of Nb with Mo, larger and larger structure defects are formed due to the decreasing energy of the entire system. The increase in Mo content also influences the increase of free volumes calculated on the basis of the DSC curves (Fig. 7). This is consistent with the indirect study of the structure by means of the approach to ferromagnetic saturation (Fig. 6, Table 3).

4. CONCLUSIONS

Interesting insights have been gained based on DSC analysis. The shapes of the DSC curves for the Nb5, Nb$_4$Mo$_1$ and Nb$_3$Mo$_2$ alloys were similar, and three exothermic minima were distinguished; the first corresponded to primary crystallization and the second and third related to secondary crystallization. Changes in the crystallization process were observed, when the quantity of Mo was greater than that of Nb in the alloy composition. In these cases, the third minimum disappeared, and the peak area corresponding to secondary crystallization widened substantially. In addition, the peak related to primary crystallization consisted of two, closely-placed, minima, related to the corresponding regions with very similar chemical composition. The decreasing values of MS are obvious effects of the introduction of Mo into the alloy, in increasing quantities. This behavior is a result of the change in the material parameter D_{spf}, which is related to interactions between the nearest-neighbor magnetic atoms. The evolution of the amorphous structure, related with the contribution of Mo and Nb, is clearly visible from analysis of the primary magnetization curves, based on H. Kronmüller's theorem of the approach to ferromagnetic saturation. It has been demonstrated that, within the volume of each sample, defects are present in the amorphous structure, the character of which depends of the chemical composition of the alloy. A gradual change in the chemical composition of the alloys leads to the collective re-distribution of the free atoms; this results in the linking of the "free volumes" into larger, though less thermodynamically stable, two-dimensional defects, in the form of quasi-dislocation dipoles. In Kaul [41] and Corb [42], it is stated that, in the relaxed amorphous structure, each magnetic atom possesses 12 neighbors, and in stressed regions, 9 to 10 neighbors. This means that a decrease in the value of the parameter D_{spf} could be related with the decreased number of nearest magnetic atoms, which leads to an improvement in the short-range chemical order. This is in agreement with the results obtained within these studies.

In conclusion, this work examined the structural and magnetic properties of rapidly-quenched Fe-based alloys. Based on analysis of the obtained results, the following conclusions were drawn:

1. The replacement of Nb with Mo reduces the values of: saturation magnetization, D_{spf} parameter and GFA parameters.
2. For the investigated alloys, and the manufacturing method used, the replacement of Nb with Mo affects the type of structural defects present in and the chemical ordering of the samples.
3. It is assumed that 5-component alloys should have higher GFA than 4-component alloys. In this case, this has not been confirmed as the best GFA is manifested by a 4-component alloy without the replacement of Nb with Mo.
4. Free volumes are an important factor influencing the magnetic properties. The paper shows that the number of free volumes calculated on the basis of DSC curves corresponds to the size of the structure defects determined on the basis of the analysis of primary magnetization curves.

REFERENCES

[1] P. Duwez, R.H. Willens, and R.C. Crewdson, "Amorphous phase in palladium – silicon alloys," *J. Appl. Phys.*, vol. 36, p. 2267, 1965, doi: 10.1063/1.1714461.
[2] W. Klement, R.H. Willens, and P. Duwez, "Non-crystalline structure in solidified gold-silicon alloys," *Nature*, vol. 187, no. 4740, pp. 869–870, 1960, doi: 10.1038/187869b0.
[3] H.S. Chen and D. Turnbull, "Formation, stability and structure of palladium-silicon based alloy glasses," *Acta Metallurgica*, vol. 17, pp. 1021–1031, 1969, doi: 10.1016/0001-6160(69)90048-0.
[4] M.E. McHenry, M.A. Willard, and D.E. Laughlin, "Amorphous and nanocrystalline materials for applications as soft magnets," *Prog. Mater. Sci.*, vol. 44, p. 291, 1999, doi: 10.1016/S0079-6425(99)00002-X.
[5] H.X. Lia, Z.C. Lua, S.L. Wang, B, Y. Wua, and Z.P. Lu, "Fe-based bulk metallic glasses: Glass formation, fabrication, properties and applications," *Prog. Mater. Sci.*, vol. 103, pp. 235–318, 2019, doi: 10.1016/j.pmatsci.2019.01.003.
[6] F. Wang *et al.*, "Excellent soft magnetic Fe-Co-B-based amorphous alloys with extremely high saturation magnetization above 1.85 T and low coercivity below 3 A/m," *J. Alloy. Compd.*, vol. 711, pp. 132–142, 2017, doi: 10.1016/j.jallcom.2017.03.341.
[7] X. Li, Z. Shi, and T. Zhang, "Effect of similar element substitution on Fe-B-Si-Mo bulk metallic glasses studied by experiment and ab initio molecular dynamics simulation," *J. Alloy. Compd.*, vol. 784, pp. 1139–1144, 2019, doi: 10.1016/j.jallcom.2019.01.122.
[8] Y. Geng *et al.*, "Formation and structure-property correlation of new bulk Fe–B–Si–Hf metallic glasses," *Mater. Des.*, vol. 106, pp. 69–73, 2016, doi: 10.1016/j.matdes.2016.05.102.
[9] Z. Jaafari, A.Seifoddini, and S.Hasani, "Enhanced mechanical and magnetic properties of [(Fe$_{0.9}$ni$_{0.1}$)$_{77}$Mo$_5$P$_9$C$_{7.5}$B$_{1.5}$]$_{99.9}$ Cu$_{0.1}$ bulk metallic glass by partial annealing," *Metall. Mater. Trans.*, vol. 50, pp. 2875–2885, 2019, doi: 10.1007/s11661-019-05195-z.
[10] Y. Han *et al.*, "FeCo-based soft magnetic alloys with high Bs approaching 1.75 T and good bending ductility," *J. Alloy. Compd.*, vol. 691, pp. 364–368, 2017, doi: 10.1016/j.jallcom.2016.08.250.
[11] K. Błoch, "Magnetic properties of the suction-cast bulk amorphous alloy: (Fe0.61Co0.10Zr0.025Hf0.025Ti0.02W0.02B0.20) 96Y4," *J. Magn. Magn. Mater.*, vol. 390, pp. 118–122, 2015, doi: 10.1016/j.jmmm.2015.04.032.
[12] J. Gondro, "Structure, core losses, curie temperature, defects in the structure of the bulk amorphous alloy Fe$_{55}$Co$_{15}$ W$_2$Y$_8$B$_{20}$," *Rev. Chim.*, vol. 70, no. 7, pp. 2699–2702, 2019, doi: 10.37358/RC.19.7.7409.
[13] P. Pietrusiewicz, M. Nabialek, J. Olszewski, and S. Lesz, "The influence of an isothermal annealing process on the structure and magnetic properties of the bulk amorphous alloy Fe-CoBYMo," *Mater. Technol.*, vol. 51, pp. 157–162, 2017, doi: 10.17222/mit.2015.151.

B. Jeż and M. Nabiałek

[14] H. Kronmüller and M. Fähnle, *Micromagnetism and the Microstructure of Ferromagnetic Solids*, Cambridge University Press: Cambrige, UK, 2003.

[15] H. Kronmüller and S. Parkin, *Handbook of Magnetism and Advanced Magnetic Materials*, Wiley: Hoboken, NJ, USA, 2007.

[16] H. Kronmüller, M. Fahnle, H. Grimm, R. Grimm, and B. Gröger, "Magnetic properties of amorphous ferromagnetic alloys," *J. Magn. Magn. Mater.*, vol. 13, p. 53, 1979, doi: 10.1016/0304-8853(79)90029-5.

[17] H. Kronmüller, "Micromagnetism in Amorphous Alloys," *IEEE Trans. Magn.*, vol. 15, p. 1218, 1979, doi: 10.1109/TMAG.1979.1060343.

[18] H. Grimm and H. Kronmüller, "Investigation of structural defects in the amorphous ferromagnetic alloy $Fe_{40}Ni_{40}P_{14}B_6$," *Phys. Status Solidi B-Basic Res.*, vol. 117, pp. 663–674, 1983, doi: 10.1002/pssb.2221170228.

[19] T. Holstein and H. Primakoff, "Magnetization near saturation in polycrystalline ferromagnets," *Phys. Rev.*, vol. 59, pp. 388–394, 1949, doi: 10.1103/PhysRev.59.388.

[20] F. Hu, C. Yuan, Q. Luo, W. Yang, and B. Shen, "Effects of Ho addition on thermal stability, thermoplastic deformation and magnetic properties of FeHoNbB bulk metallic glasses," *J. Alloy. Compd.*, vol. 807, p. 151675, 2019, doi: 10.1016/j.jallcom.2019.151675.

[21] T. Qi, Y. Li, A. Takeuchi, G. Xie, H. Miao, and W. Zhang, "Soft magnetic Fe25Co25Ni25(B, Si)25 high entropy bulk metallic glasses," *Intermetallics*, vol. 66, pp. 8–12, 2015, doi: 10.1016/j.intermet.2015.06.015.

[22] A. Takeuchi and A. Inoue, "Classification of bulk metallic glasses by atomic size difference, heat of mixing and period of constituent elements and its application to characterization of the main alloying element," *Mater. Trans.*, vol. 46, pp. 2817–2829, 2005, doi: 10.2320/matertrans.46.2817.

[23] T. Nagase, M. Suzuki, and T. Tanaka, "Amorphous phase formation in Fe–Ag-based immiscible alloys," *J. Alloy. Compd.*, vol. 619, pp. 311–318, 2015, doi: 10.1016/j.jallcom.2014.08.212.

[24] A. Inoue, "Bulk amorphous alloys with soft and hard magnetic properties," *Mater. Sci. Eng. A*, vol. 226–228, pp. 357–363, 1979, doi: 10.1016/S0921-5093(97)80049-4.

[25] E.R. Shaaban and I.B.I. Tomsah, "The effect of Sb content on glass-forming ability, the thermal stability, and crystallization of Ge–Se chalcogenide glass," *J. Therm. Anal. Calorim.*, vol. 105, pp. 191–198, 2011, doi: 10.1007/s10973-011-1317-z.

[26] E. Civan, K. Sarlar, and I. Kucuk, "Improving magnetocaloric properties of Fe68-xCrxTb5B23Nb4 (x=0, 2, 4, 6 and 8) metallic glasses having high glass-forming ability with tunable Curie temperature," *Philos. Mag.*, vol. 97, pp. 1464–1478, 2017, doi: 10.4283/jmag.2019.24.1.043.

[27] B. Wunderlich, Y. Jin, and A. Boller, "Mathematical description of differential scanning calorimetry based on periodic temperature modulation," *Thermochim. Acta*, vol. 238, pp. 277–293, 1994, doi: 10.1016/S0040-6031(94)85214-6.

[28] A. Inoue, "High Strength Bulk Amorphous Alloys with Low Critical Cooling Rates," *Mater. Trans. JIM*, vol. 36, pp. 866–875, 1995, doi: 10.2320/matertrans1989.36.866.

[29] D. Turnbull, "Under what conditions can a glass be formed," *Contemp. Phys.*, vol. 10, pp. 473–488, 1969, doi: 10.1080/00107516908204405.

[30] Z.P. Lu and C.T. Liu, "A new glass-forming ability criterion for bulk metallic glasses," *Acta Mater.*, vol. 50, pp. 3501–3512, 2002, doi: 10.1016/S1359-6454(02)00166-0.

[31] Q. Chen, J. Shen, D. Zhang, H. Fan, J. Sun and D. McCartney, "A new criterion for evaluating the glass-forming ability of bulk metallic glasses," *Mater. Sci. Eng. A*, vol. 433, pp. 155–160, 2006, doi: 10.1016/j.msea.2006.06.053.

[32] P. Rezaei-Shahreza, A. Seifoddini, and S. Hasani, "Thermal stability and crystallization process in a Fe-based bulk amorphous alloy: The kinetic analysis," *J. Non-Cryst. Solids*, vol. 471, pp. 286–294, 2017, doi: 10.1016/j.jnoncrysol.2017.05.044.

[33] Z. Jaafari, A. Seifoddoni, S. Hasani, and P. Rezaei-Shahreza, "Kinetic analysis of crystallization process in [(Fe0. 9Ni0. 1) 77Mo5P9C7. 5B1. 5] 100− xCux (x= 0.1 at.%) BMG," *J. Therm. Anal. Calorim.*, vol. 134, pp. 1565–1574, 2018, doi: 10.1007/s10973-018-7372-y.

[34] H.E. Kissinger, "Reaction kinetics in differential thermal analysis," *Anal. Chem.*, vol. 29, pp. 1702–1706, 1957, doi: 10.1021/ac60131a045.

[35] K.S. Dubey and P. Ramchandrarao, "On the free energy change accompanying crystallisation of undercooled melts," *Acta Metall.*, vol. 32, pp. 91, 1984, doi: 10.1016/0001-6160(84)90205-0.

[36] M. Shi, Z. Liu, and T. Zhang, "Effects of minor Sn addition on the glass formation and properties of Fe-metalloid metallic glasses with high magnetization and high glass forming ability," *J. Magn. Magn. Mater.*, vol. 378, pp. 417–423, 2015, doi: 10.1016/j.jmmm.2014.10.144.

[37] L. Battezzati and E. Garrone, "On the approximation of the free energy of undercooled glass-forming metallic melts," *Zeitschrift-fuer Metallkunde*, vol. 75, pp. 305–310, 1984, doi: 10.1515/ijmr-1984-750410.

[38] C. Qing-Jun, S. Jun, F. Hong-Bo, S. Jian-Fei, and H. Yong-Jiang, "Glass-forming ability of an iron-based alloy enhanced by Co addition and evaluated by a new criterion," *Chin. Phys. Lett.*, vol. 22, pp. 1736–1738, 2005.

[39] S. Hasani, P. Rezaei-Shahreza, A.Seifoddini, and A. Hakimi, "Enhanced glass-forming ability, mechanical, and magnetic properties of Fe41Co7Cr15Mo14Y2C15B6 bulk metallic glass with minor addition of Cu," *J. Non-Cryst. Solids*, vol. 497, pp. 40–47, 2018, doi: 10.1016/j.jnoncrysol.2018.05.021.

[40] X. Li and T. Zhang, "Correlation between local structure and glass forming ability enhanced by similar element substitution in (La-Ce)-Co-Al bulk metallic glasses," *J. Appl. Phys.*, vol. 122, pp. 85103, 2017, doi: 10.1063/1.4998437.

[41] N. Kaul, "Magnetic properties of amorphous (Fe, Ni)80B20, (Fe, Ni)80B19si1, and (Fe, Ni)80P14B6 alloys," *IEEE Trans. Magn.*, vol. 17, pp. 1208–1215, 1981, doi: 10.1109/TMAG.1981.1061194.

[42] B.W. Corb, R.C.O'Handley, and N.J. Grant, "Chemical bonding, magnetic moments, and local symmetry in transition-metal – Metalloid alloys," *Phys. Rev. B*, vol. 27, p. 636, 1983, doi: 10.1103/PhysRevB.27.636.